JOURNAL OF MATERIALS SCIENCE 35 (2000) 4031–4037

N_2O decomposition over $(Mg_{6-x}A_x)MnO_8$ (A = Li, Al)

K. TABATA*, T. KARASUDA, E. SUZUKI
Research Institute of Innovative Technology for the Earth (RITE) Kizugawadai, Kizu-cho, Soraku-gun, Kyoto, 619-0292 Japan
E-mail: kenjt@rite.or.jp

H. TAGUCHI
Research Laboratory for Surface Science, Faculty of Science, Okayama University, Okayama 700, Japan

Two different murdochite-type mixed oxides, $(Mg_{6-x}Li_x)MnO_8$ ($x = 0$, 0.1, 0.2 and 0.3) and $(Mg_{6-x}Al_x)MnO_8$ ($x = 0$, 0.2, 0.4, 0.6) were examined for the catalytic decomposition of N_2O in order to make clear the effects of mixed valencies of pairing manganese ions and oxygen vacancies. The valence of manganese ions and the amount of surface oxygen vacancies have been examined with X-ray photoelectron spectroscopy (XPS). $(Mg_{6-x}Li_x)MnO_8$ had mixed valence manganese ions and oxygen vacancies on the surface after the substitution. The substituted $(Mg_{6-x}Al_x)MnO_8$ had a mixed valence state but oxygen vacancies decresed with x and excess oxygen over stoichiometry was observed at $x = 0.4$ and 0.6. The reaction rate of N_2O decomposition increased after substitution with lithium but hardly increased after the substitution with aluminum in $(Mg_{6-x}A_x)MnO_8$. We assumed that the presence of oxygen vacancies on the surface along with pairing altervalent manganese ions affected strongly to enhance the reactivity of N_2O decomposition. © *2000 Kluwer Academic Publishers*

1. Introduction

Since N_2O has been identified as a contributor to the destruction of ozone in the stratosphere and recognized as a relatively strong greenhouse gas, N_2O has been focused intensively [1, 2]. N_2O decomposition has been studied over metals, metal oxides and some zeolites [3–7]. Pure oxides have been examined and the transition metal oxides of group VIII (Rh, Ir, Co, Fe, Ni) and CuO and La_2O_3 showed high reactivities [4]. In these experiments, the variations of the valency of active elements affected strongly on the reactivities. Yamashita *et al.* examined the decomposition of N_2O over four different manganese oxides but stable behavior was observed only for Mn_2O_3 and Mn_3O_4 [7]. The activity of Mn_2O_3 was higher than that of Mn_3O_4 at 350 °C.

Perovskite-related structures which are controllable with oxygen defects and valencies of metal ions have collected many studies [5, 6]. Raj *et al.* examined the substitution effects on N_2O decomposition with $La_{1-x}Sr_xMnO_3$ [8]. They examined the variation of apparent activation energy and that of Mn^{4+} atomic % as a function of the fraction of Sr in $La_{1-x}Sr_xMnO_3$. The optimal activity was found where the Mn^{3+}/Mn^{4+} ratio was 1 : 1. Wan *et al.* examined the catalytic decomposition of N_2O over $La_{2-x}Sr_xCuO_3$ ($x = 0$-1) [5]. The optimum average oxidized number of copper for the activity was 2.3 at $x = 0.5$. They explained the variation of catalytic activities by a Cu^{2+}/Cu^{3+} redox mechanism.

Murdochite-type Mg_6MnO_8 is derived from the rock-salt structure of MgO by the replacement of one-eighth with vacancies [9, 10]. In the previous paper, we synthesized $(Mg_{6-x}Al_x)MnO_8$ ($0.0 \leq x \leq 0.6$) by substituting Al^{3+} ion for Mg^{2+} ion in Mg_6MnO_8 [11]. From the variations of the cell constants and the magnetic properties, we reported that $(Mg_{6-x}Al_x)MnO_8$ had the mixed valencies of Mn^{3+} and Mn^{4+} ions. We synthesized also $(Mg_{6-x}Li_x)MnO_8$ ($0.0 \leq x \leq 0.3$) and examined the crystal structure and the magnetic properties [12]. We assured the coexistence of Mn^{4+} and Mn^{5+} ions from the variation of the effective magnetic moments.

In this study, the variations of reactivities of $(Mg_{6-x}A_x)MnO_8$ (A = Al or Li) for N_2O decomposition were examined in order to clear the effects of coexistent mixed valencies of manganese ions. The valence of manganese ions on the surface was examined with XPS because the decomposition of N_2O was suggested to be a suprafacial reaction [6]. The effects of presence of oxygen vacancies on the surface of $(Mg_{6-x}A_x)MnO_8$ (A = Al or Li) for N_2O decomposition will be also discussed.

* Author to whom all correspondence should be addressed.

2. Experimental

2.1. Materials

$(Mg_{6-x}Li_x)MnO_8$: $Mg(CH_3COO)_2{\cdot}4H_2O$, $Mn(CH_3COO)_2{\cdot}4H_2O$, $Li(CH_3COO){\cdot}2H_2O$ were weighted in the appropriate proportions and mixed with acetone. The mixed powders were dried and calcined at 400 °C for 2 h in the flow of pure oxygen gas, then calcined at 700 °C for 6 h in the flow of pure oxygen gas.

$(Mg_{6-x}Al_x)MnO_8$: $Mg(CH_3COO)_2{\cdot}4H_2O$, $Mn(CH_3COO)_2{\cdot}4H_2O$ and $Al(NO_3)_3{\cdot}9H_2O$ were weighted in the appropriate proportions and dissolved in distilled water at room temperature. The solution was mixed and evaporated in a rotary evaporator at 40–60 °C, and the obtained gel was calcined at 400 °C for 2 h in the air, then calcined at 700 °C for 6 h in the air.

2.2. Characterization

The phases of the samples were identified with a powder X-ray diffractometer with monochromatic Cu K_α radiation. The crystallite size (D_{400}) of the samples was calculated from the half-width of a diffraction peak at (400) with Scherrer's equation [13]. BET specific surface area of the samples was measured with N_2 adsorption at 77 K. XPS experiments were performed with ESCA 3200 spectrometer (Shimadzu Co.). Mg K_α (1253.6 eV) X-ray source was used for the excitation. The spectrometer worked under a base pressure of 1×10^{-6} Pa in a chamber. The sample was indirectly heated by a resistivity heater. Binding energy (BE) was calibrated with respect to the value of the C 1s level of a contaminated carbon as 285.0 eV. Photoelectron was detected at the angle of 45° to the surface of a sample. The treatment of acquired spectrum was carried out with the software "Vision" produced by Kratos Analytical. The atomic ratio was calculated from each spectrum area with its sensitivity factor by Wagner [14]. Pass energy was 75 eV.

The bulk composition was measured with an inductively coupled plasma atomic emission spectroscopy (ICP-AES). The amount of oxygen in a sample was calculated from the differences between total sample weight and measured total weight percentages of other elements.

2.3. Test reaction

The catalytic activity for N_2O decomposition was measured at 400–700°C with a conventional flow system. The samples (0.10 g) were preheated at 300°C in a pure oxygen gas for 2 h. The mixed gas of N_2O (3.0%) and He (balance) was fed in the flow reactor at the flow rate of 150 cm^3/min. The product was analyzed with a gas chromatography (molecular sieve 5A) kept at 50 °C.

3. Results

Powder X-ray diffraction patterns of $(Mg_{6-x}Li_x)MnO_8$ were completely indexed as a cubic murdochite type structure in the range of $x = 0.0$ to 0.3. The crystallite size (D_{400}) of the samples was calculated and the result was shown in Table I. The D_{400} value of $(Mg_{6-x}Li_x)MnO_8$ increases from 76.7 nm ($x = 0.0$) to 128 nm ($x = 0.3$). The specific surface area (S) of the sample was also shown in Table I. The specific surface area decreases from 14.7 m^2/g ($x = 0.0$) to 5.2 m^2/g ($x = 0.3$) with x.

TABLE I Crystallite size (D_{400}) and specific surface area (S) of $(Mg_{6-x}Li_x)MnO_8$ and $(Mg_{6-x}Al_x)MnO_8$

x in $(Mg_{6-x}Li_x)MnO_8$	D_{400} (nm)	S (m^2/g)
0.0	76.7	14.7
0.1	103	8.1
0.2	117	6.3
0.3	128	5.2
x in $(Mg_{6-x}Al_x)MnO_8$	D_{400} (nm)	S (m^2/g)
0.0	76.7	14.7
0.2	61.0	26.6
0.4	49.7	34.9
0.6	47.1	35.0

The temperature dependence of the rate of N_2O decomposition for $(Mg_{6-x}Li_x)MnO_8$ is shown in Fig. 1. The activities increased in the range over 600 °C, and each rate from $x = 0$ to $x = 0.3$ increased in proportion to the substitution quantity, x. We examined the bulk and the surface composition of a sample with ICP-AES and XPS respectively. The results were shown in Table II. The results of measured bulk composition reproduced well our expected values on the preparation. Concerning a sample treatment for XPS measurements, the sample was heated at 400 °C for 1 h in a vacuum chamber for removing hydroxyl ion species and contaminations from the surface. XPS measurements were carried out at room temperature. No other elements than expected ones (Mg, Li, Mn, O) and a slight carbon were observed in every spectrum. In the previous paper, we reported that the manganese ions in the bulk of $(Mg_{6-x}Li_x)MnO_8$ coexisted as Mn^{4+} and Mn^{5+} from the variation of effective magnetic moments. We examined the valency of manganese ions on the surface of $(Mg_{6-x}Li_x)MnO_8$ with XPS because manganese ions were assumed to be active sites. The values of peak

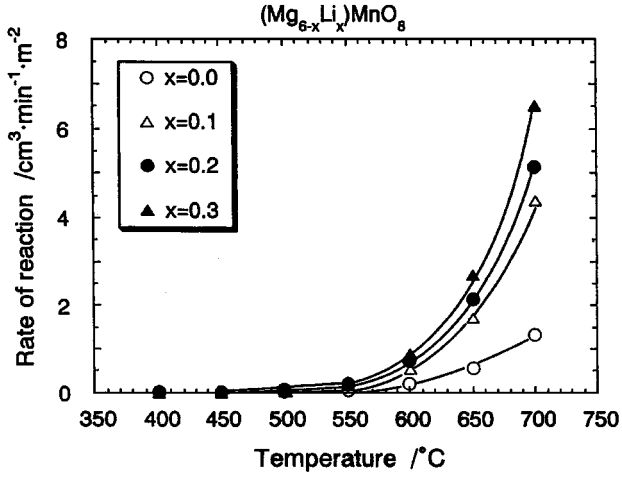

Figure 1 The reaction rate of N_2O decomposition for $(Mg_{6-x}Li_x)MnO_8$ from $x = 0$ to $x = 0.3$.

TABLE II The observed bulk composition of $(Mg_{6-x}Li_x)MnO_8$ and $(Mg_{6-x}Al_x)MnO_8$ measured with ICP-AES. The observed formal surface compositional formula and surface oxygen vacancy (Vö) measured with XPS

x in $(Mg_{6-x}Li_x)MnO_8$	Bulk Composition	Surface Composition	Vö
0.0	$Mg_6MnO_{8.4}$	$Mg_6MnO_{7.6}$	0.4
0.1	$Mg_{5.9}Li_{0.1}MnO_{8.4}$	$Mg_{5.4}Li_{0.01}Mn_{0.6}O_{6.0}$	0.6
0.2	$Mg_{5.8}Li_{0.2}MnO_{8.4}$	$Mg_{5.8}Li_{0.2}Mn_{1.0}O_{7.0}$	1.0
0.3	$Mg_{5.8}Li_{0.3}MnO_{8.3}$	$Mg_{5.6}Li_{0.1}Mn_{0.8}O_{4.8}$	2.5
x in $(Mg_{6-x}Al_x)MnO_8$	Bulk Composition	Surface Composition	Vö
0.0	$Mg_{6.0}MnO_{8.4}$	$Mg_6MnO_{7.6}$	0.4
0.2	$Mg_{5.9}Al_{0.2}MnO_{10.0}$	$Mg_{4.3}Al_{3.6}Mn_{0.6}O_{10.8}$	0.2
0.4	$Mg_{5.6}Al_{0.4}MnO_{10.7}$	$Mg_{4.3}Al_{3.8}Mn_{0.6}O_{5.4}$	-2.2^*
0.6	$Mg_{5.4}Al_{0.6}MnO_{11.0}$	$Mg_{3.4}Al_{4.6}Mn_{0.6}O_{6.2}$	-1.8^*

*: Minus represents excess oxygen over the stoichiometry.

position of the Mn $2p_{3/2}$ level and the full width at half maximum (FWHM) are listed in Table III, and the spectra for the Mn 2p level are shown in Fig. 2. The peak position of Mn^{4+} ions in MnO_2 for the Mn $2p_{3/2}$ level has been reported as 642.4–642.8 eV. [15, 16]. The observed peak positions of $(Mg_{6-x}Li_x)MnO_8$ were 642.9–643.1 eV. The values of FWHM were 2.4–3.1 eV and these values seem to be larger than that for one species. Our observed peak positions of the samples were a little bit higher than the reported ones for Mn^{4+} in MnO_2. The observed peak position of every sample for the Mn $2p_{3/2}$ level is almost the same, and the values of FWHM decreased slightly after substitution with Li. We therefore assumed the valency of manganese ions on the surface was a mixed valency state. One of the mixed valency could be Mn^{4+} but other valencies of manganese ions were not clear whether Mn^{5+} observed in the bulk presented on the surface or not.

Fig. 3 shows the spectra for the O 1s level. Every spectrum could be resolved to two peaks. The resolved

TABLE III The peak positions and FWHM values of Mn $2p_{3/2}$ level spectra for $(Mg_{6-x}Li_x)MnO_8$ and $(Mg_{6-x}Al_x)MnO_8$ measured with XPS

	Mn $2p_{3/2}$	
x in $(Mg_{6-x}Li_x)MnO_8$	Peak position (eV)	FWHM (eV)
0.0	643.1	3.1
0.1	642.9	2.4
0.2	643.0	2.9
0.3	642.9	2.8
	Mn $2p_{3/2}$	
x in $(Mg_{6-x}Al_x)MnO_8$	Peak position (eV)	FWHM (eV)
0.0	643.1	3.1
0.2	643.2	3.5
0.4	642.8	3.5
0.6	640.9	3.6

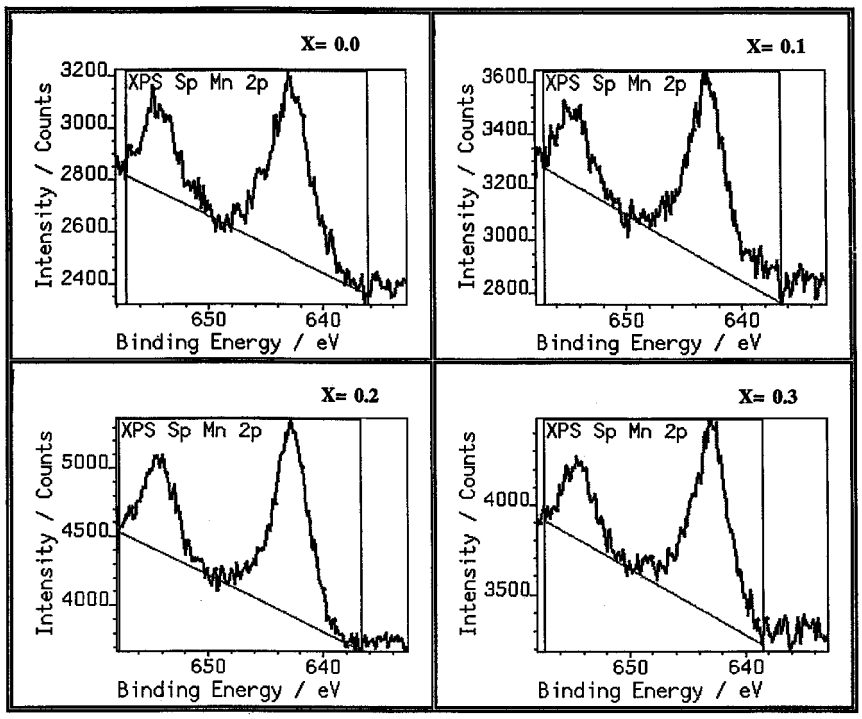

Figure 2 The Mn 2p level spectrum for $(Mg_{6-x}Li_x)MnO_8$ from $x = 0$ to $x = 0.3$.

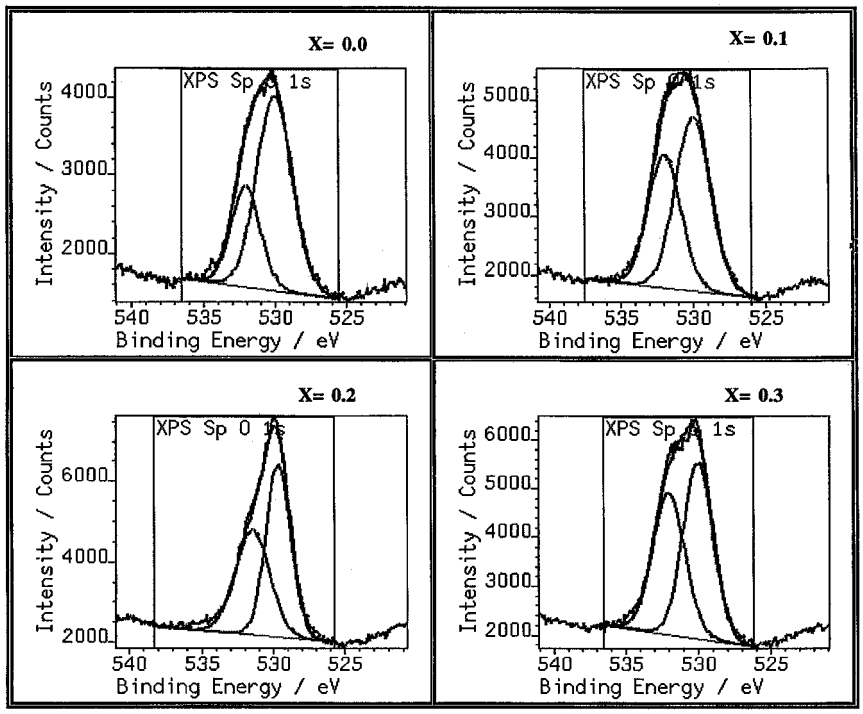

Figure 3 The resolved O 1s level spectrum for $(Mg_{6-x}Li_x)MnO_8$ from $x = 0$ to $x = 0.3$.

peaks were adjusted to fit the original one with the software. The oxygen species around about 530.0 eV is the lattice oxygen O^{2-} on the surface [17]. The peak positions of the chemisorbed oxygen species such as O^-, and O_{2-} and O_2^{2-} have been reported as around 531–533 eV [17]. The peak of the hydroxyl ion species appears at the same region [17], however, the contribution of that could be small because every sample was preheated at 400 °C for 1 h in a vacuum chamber. We considered that the chemisorbed oxygen species will desorb from the surface under a high temperature region of the reaction. We therefore calculated the atomic concentration of lattice oxygen with the sensitivity factor, and we showed the calculated formal surface compositional formulae in Table II. The obtained formula at $x = 0.0$ is $Mg_6MnO_{7.6}$, and this is close to its bulk composition. The quantity of the surface oxygen vacancy (Vö) was calculated from the obtained formal surface compositional formulae. The calculation was carried out as follows:

$$\text{Vö} = 2 \times C_{\text{Mg}} + 4 \times C_{\text{Mn}} - 2 \times C_{\text{O}} \qquad (1)$$

where C is each observed compositional proportion in Table II. Manganese ion was calculated as Mn^{4+}. The results are shown in Table II. The values oxygen vacancies on the surface increased with x.

3.1. $(Mg_{6-x}Al_x)MnO_8$ $(0.0 \leq x \leq 0.6)$

Powder x-ray diffraction patterns of $(Mg_{6-x}Al_x)MnO_8$ were completely indexed as the cubic murdochite-type structure in the range of $x = 0.0$ to 0.6. The calculated crystallite size (D_{400}) of the samples decreased as shown in Table I. The specific surface area (S) increased as opposed to the case of Li. The temperature

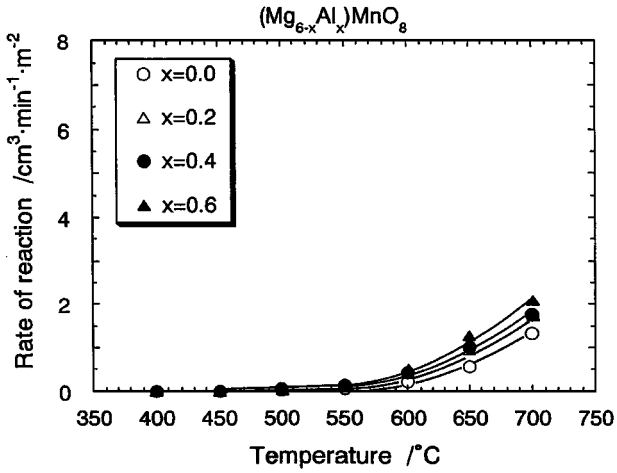

Figure 4 The reaction rate of N_2O decomposition for $(Mg_{6-x}Al_x)$-MnO_8 from $x = 0$ to $x = 0.3$.

dependence of the reaction rate of N_2O decomposition for $(Mg_{6-x}Al_x)MnO_8$ is shown in Fig. 4. The reaction rate gradually increases in the range over 600°C and the differences among $x = 0.0$–0.6 are quite small.

The observed proportions among Mg, Al and Mn in the bulk were in accord with the proportions on the preparation as shown in Table II. Concerning the amount of oxygen, excess oxygen over stoichiometry was observed after substitution.

We examined the valence state of manganese ions and the amount of oxygen vacancies on the surface of $(Mg_{6-x}Al_x)MnO_8$ as shown in Table II. The samples were preheated at 400 °C for 1h in the vacuum chamber. XPS measurements were carried out at room temperature. Any other elements except for Mg, Mn, Al, O and a slight carbon were not observed in every spectrum. Fig. 5 shows the spectra for the Mn 2p level. The

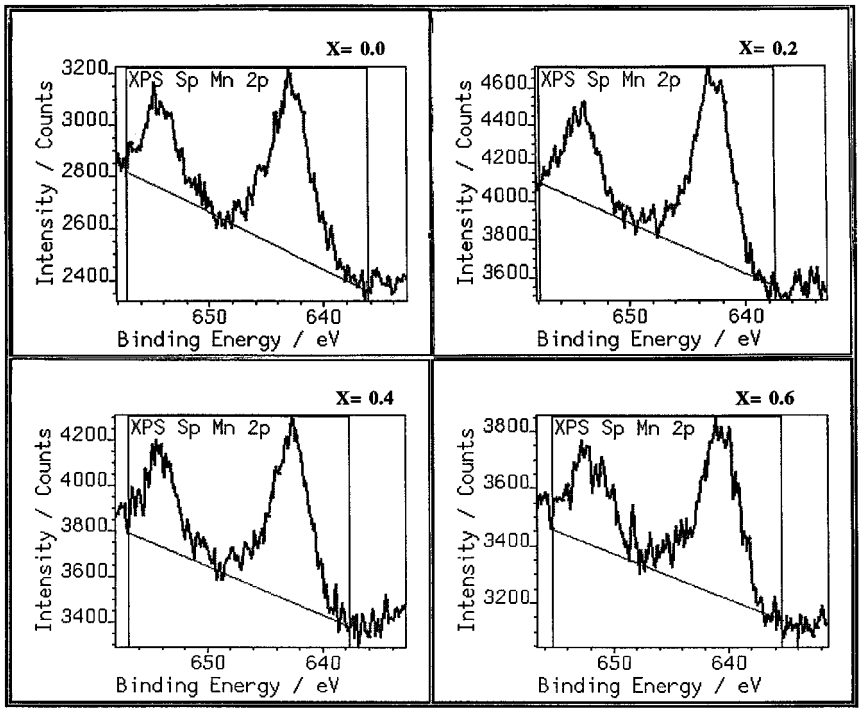

Figure 5 The Mn 2p level spectrum for $(Mg_{6-x}Al_x)MnO_8$ from $x = 0$ to $x = 0.3$.

observed peak positions and the FWHM values for the Mn $2p_{3/2}$ level are listed in Table III. The peak position of the samples for the Mn $2p_{3/2}$ level decreased from 643.1 to 640.9 eV at $x = 0.6$. We previously reported that $(Mg_{6-x}Al_x)MnO_8$ had mixed valencies of Mn^{3+} and Mn^{4+} ions in the bulk from the results of the variations of the cell constants and the magnetic properties [11]. We examined the valency state of manganese ions on the surface. The binding energies of peak positions of the Mn $2p_{3/2}$ level of α-Mn_2O_3 and β-MnO_2 were reported to be very close such as 641.9 and 642.2 eV [16]. The splitting between the Mn $2p_{3/2}$ and Mn $2p_{1/2}$ levels of these oxides was reported to be the same value, 11.6 eV [16]. Therefore it seems to be difficult to discern between Mn^{4+} and Mn^{3+} ions in the Mn 2p level spectra. The peak position of the Mn $2p_{3/2}$ level of MnO is 640.6 eV. One feature of the spectrum of MnO is the satellite peaks associated with Mn $2p_{3/2}$ and Mn $2p_{1/2}$ peaks [16]. Mn^{2+} ions in $MnCr_2O_4$ has the same satellite peaks associated with Mn $2p_{3/2}$ and Mn $2p_{1/2}$ peaks [18]. We assumed the presence of mixed valence state among Mn^{4+}, Mn^{3+} and even Mn^{2+} ions from the shift of the peak position from 643.2 to 640.9 eV and the appearance of the satellite peaks associated with Mn $2p_{3/2}$ and Mn $2p_{1/2}$ peaks in the spectra of $x = 0.2$ and 0.3. Furthermore, the large values of FWHM suggest the presence of mixed valence state.

The observed formal surface compositional formula of $(Mg_{6-x}Al_x)MnO_8$ are listed in Table II where the oxygen atomic concentration was calculated from the resolved spectra of lattice oxygen of the murdochite type mixed oxide and Al_2O_3 because the segregation of aluminum on the surface was clearly observed for the every substituted samples. Fig. 6 shows the spectra for the O 1s level of $(Mg_{6-x}Al_x)MnO_8$. We resolved every spectrum to three peaks except for that at $x = 0.0$ because the peak position of the O 1s level of the lattice oxygen for Al_2O_3 was reported as 531.2 eV [19]. We assigned each resolved peak to the lattice oxygen species of murdochite-type mixed oxide (530.0 eV) and Al_2O_3 (531.5 eV) and chemisorbed oxygen species (533.5 eV). We showed the calculated formal surface compositional formulae in Table II. The surface oxygen vacancies were calculated from the formal surface compositional formulae, and listed in Table II. The calculation of amount of surface oxygen vacancies were carried out as follows:

$$V\ddot{o} = 2 \times C_{Mg} + 4 \times C_{Mn} + 3 \times C_{Al} - 2 \times C_O \quad (2)$$

where C is each observed compositional proportion in Table II. Manganese ion was calcualted as Mn^{4+}. The oxygen vacancies were decreased with x and excessive oxygen on the surface composition was observed at $x = 0.4$ and 0.6 as shown in Table II.

4. Discussion

The catalytic decomposition of N_2O starts from the adsorption of N_2O on the active center, usually a coordinatively unsaturated surface transition metal ion, followed by a decomposition giving formation of N_2 and a surface oxygen. This surface oxygen can desorb by combination with another oxygen atom or by direct reaction with another N_2O. These four steps are written as follows:

$$N_2O + * \leftrightarrow N_2O^* \quad (3)$$

$$N_2O^* \rightarrow N_2 + O^* \quad (4)$$

$$2O^* \leftrightarrow O_2 + 2^* \quad (5)$$

$$N_2O + O^* \rightarrow N_2 + O_2 + ^* \quad (6)$$

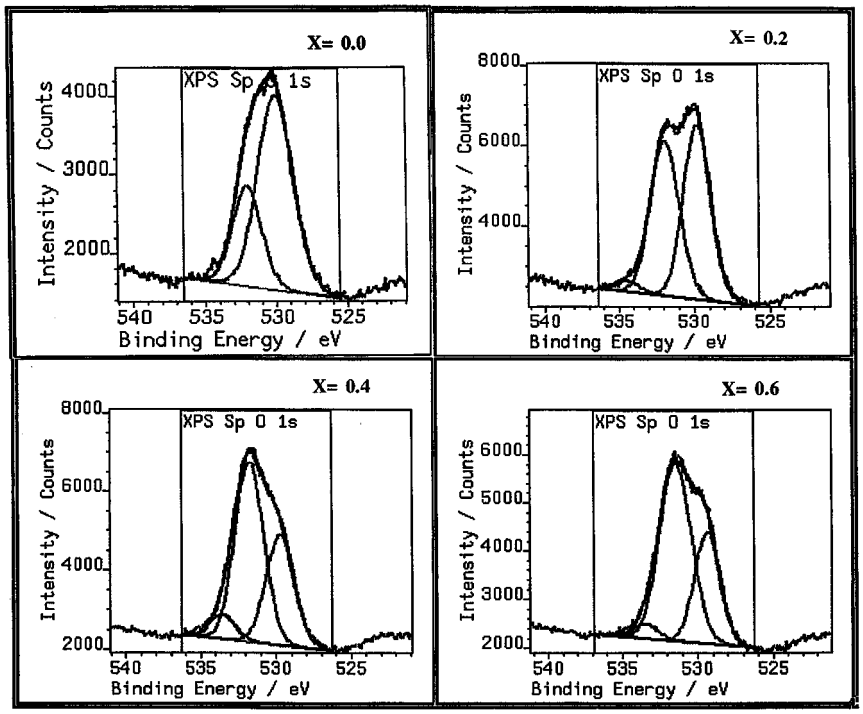

Figure 6 The resolved O 1s level spectrum for $(Mg_{6-x}Al_x)MnO_8$ from $x = 0$ to $x = 0.3$.

where * represents an active site on a surface. Equations 3 and 5 may be reversible, while Equations 4 and 6 may be irreversible. Concerning active element for the N_2O decomposition over Mg_{6-x}(Li or Al)$_x MnO_8$, manganese ion is assumed to be active element among the compositional elements [3]. The start of reaction of N_2O decomposition on the active centers of a catalyst is generally envisaged as a charge donation from the catalyst into the antibonding orbitals of N_2O, destabilising the N - O bond and leading to scission. Metal oxides with some local charge donation properties and isolated transition metal ions with more than one valency can act as such centers. In Table III, we assured the presence of mixed valence of manganese ions on the surface of $(Mg_{6-x}Li_x)MnO_8$ because the values of FWHM were comparatively larger such as 3.1–2.4 eV. The presence of Mn^{4+} ions was assumed but that of Mn^{5+} observed in the bulk was not clear.

We carried out the estimation concerning the oxygen vacancies from the observed formal surface compositional formula measured with XPS as shown in Table II. The surface oxygen vacancies of $(Mg_{6-x}Li_x)MnO_8$ increased with x. The reactivities of $(Mg_{6-x}Li_x)MnO_8$ increased with x as shown in Fig. 1. Contrary to this, the reactivity of $(Mg_{6-x}Al_x)MnO_8$ was hardly increased with x and the difference of reactivities was small at even 700 °C as shown in Fig. 4. $(Mg_{6-x}Al_x)MnO_8$ has a mixed valence state of manganese ions as assured from the values of FWHM and the Mn 2p level spectra. The oxygen vacancies on the surface of $(Mg_{6-x}Al_x)MnO_8$ decreased with x. Even excess oxygen over the stoichiometries were obtained for the samples at $x = 0.4$ and 0.6 as shown in Table III. The pairing of different valencies on the surface manganese ions was observed for both $(Mg_{6-x}Li_x)MnO_8$ and $(Mg_{6-x}Al_x)MnO_8$. The pairing site was assumed to constitute an active site for the reaction because the pairing site seems to make easier the optimal charge transfers, from a metal ion to N_2O upon facilitation of N-O bonding and back from a formed surface oxygen to active metal ion upon desorption by the exchange of an electron between two different oxidized metal ions through the O 2p orbital. However, the reactivity of $(Mg_{6-x}Li_x)MnO_8$ which has mixed valency on the surface was hardly enhanced even after the substitution at $x = 0.6$. We therefore assumed the presence of anion vacancies along with the pairing cations was important to enhance the reactivity of N_2O decomposition.

5. Conclusions

We prepared two different murdochite-type mixed oxides, i.e. $(Mg_{6-x}Li_x)MnO_8$ and $(Mg_{6-x}Al_x)MnO_8$. The activities of N_2O decomposition were examined. The valence state of manganese ion on the surface and surface oxygen vacancies were examined with XPS. $(Mg_{6-x}Li_x)MnO_8$ had the oxygen vacancie and the amount of those increased with x. The valence state of manganese ions are assumed to be a mixed valency state from the value of FWHM. The presence of mixed valence state of Mn^{4+}, Mn^{3+} and Mn^{2+} for the surface manganese ions in $(Mg_{6-x}Al_x)MnO_8$ was observed from the spectra of the Mn $2p_{3/2}$ level and the values of FWHM. Oxygen vacancies on the surface of $(Mg_{6-x}Al_x)MnO_8$ were not observed after the substitution. The presence of pairing cations along with the surface oxygen vacancies in $(Mg_{6-x}Li_x)MnO_8$ enhanced the reactivities of N_2O decomposition. However, the presence of the mixed valence manganese ions without oxygen vacancies in $(Mg_{6-x}Al_x)MnO_8$ affected little on the reactivities. We assumed that the presence of oxygen vacancies along with pairing cations with different valencies affected strongly on the reactivity of N_2O decomposition.

Acknowledgements

This work was financially supported by the New Energy and Industrial Technology Development Organization (NEDO, Japan).

References

1. J. C. KRAMLICH and W. P. LINAK, *Prog. Energy Combust. Sci.* **20** (1994) 149.
2. M. A. WOJTOWICZ, J. R. PELS and J. A. MOULIJN, *Fuel Proc. Technol.* **34** (1993) 1.
3. F. KAPTEIJN, J. R. MIRASOL and J. A. MOULIJN, *Appl. Catal. B* **9** (1996) 25.
4. G. I. GOLODETS, *Stud. Surf. Sci. Cat.* **15** (1983) 200.
5. J. WANG, H. YASUDA, K. INUMARU and M. MISONO, *Bull. Chem. Soc. Jpn.* **68** (1995) 1226.
6. C. S. SWAMY and J. CHRISTOPHER, *Catal. Rev. -Sci. Eng.* **34** (1992) 409.
7. T. YAMASHITA and A. VANNICE, *J. Catal.* **161** (1996) 254.
8. S. L. RAJ, B. VISWANATHAN and V. SRINIVASAN, *ibid.* **75** (1982) 185.
9. J. S. KASPER and J. S. PRENER, *Acta Crystallogr.* **7** (1954) 246.
10. P. PORTA and M. VALIGI, *J. Solid State Chem.* **6** (1973) 344.
11. H. TAGUCHI, A. OKAMOTO, M. NAGAO and H. KIDO, *ibid.* **102** (1993) 570.
12. H. TAGUCHI, A. OHTA, M. NAGAO, H. KIDO, H. ANDO and K. TABATA, *ibid.* **124** (1996) 220.
13. B. D. CULLITY, "Elements of X-ray Diffraction" (Addison-Weley, London, 1978) p. 102.
14. C. D. WAGNER, *Anal. Chem.* **49** (1977) 1282.
15. *Idem.*, "Practical Surface Analysis" (John Wiley & Sons, New York, 1995) p. 595.
16. M. OKU, K. HIROKAWA and S. IKEDA, *J. Electron Spectrosc. Relat. Phenom.* **7** (1995) 465.
17. M. CHE and A. J. TENCH. *Adv. Catal.* **32** (1983) 1.
18. M. OKU and K. HIROKAWA, *J. Electron Spectrosc. Relat. Phenom.* **8** (1976) 475.
19. T. L. BARR, "Modern ESCA" (CRC Press, Boca Raton, 1994) p. 186.

Received 27 August 1999
and accepted 22 February 2000